Energy & Environmental Science

COMMUNICATION

View Article Online
View Journal

Cite this: DOI: 10.1039/c9ee02311a

Received 22nd July 2019,
Accepted 19th August 2019

DOI: 10.1039/c9ee02311a

rsc.li/ees

Air-stable Li_3InCl_6 electrolyte with high voltage compatibility for all-solid-state batteries†

Xiaona Li,‡[a] Jianwen Liang,‡[a] Jing Luo,[a] Mohammad Norouzi Banis,[ab] Changhong Wang,[a] Weihan Li,[ac] Sixu Deng,[a] Chuang Yu,[a] Feipeng Zhao,[a] Yongfeng Hu,[b] Tsun-Kong Sham,[c] Li Zhang,[d] Shangqian Zhao,[d] Shigang Lu,[d] Huan Huang,[e] Ruying Li,[a] Keegan R. Adair[a] and Xueliang Sun *[a]

Most inorganic solid-state electrolytes (SSEs) suffer from incompatibility with oxide cathode materials and instability in ambient air, presenting major barriers for their application in high performance all-solid-state batteries (ASSLBs). Herein, we report a rationally designed halide-based Li_3InCl_6 SSE with a high ionic conductivity of 1.49×10^{-3} S cm^{-1} (25 °C). The Li_3InCl_6 SSE is stable towards oxide cathode materials (*e.g.*, $LiCoO_2$) without any interfacial treatment. By applying the Li_3InCl_6 SSEs, significantly enhanced electrochemical performances are achieved in terms of capacity and durability. Experimental investigations reveal that the Li_3InCl_6 can avoid side reactions between the SSEs and the oxide cathode materials and thus effectively improve the Li^+ migration across the interface. Moreover, Li_3InCl_6 is highly stable in ambient air and possesses good ionic conductivity retention after a reheating process, further making it an attractive electrolyte for next-generation ASSLBs.

Broader context

Solid-state-electrolytes (SSEs) are key materials in all-solid-state lithium batteries because the properties of the batteries highly depend on the characteristics of the SSEs. However, currently developed SSEs still fall short of one or more practical requirements including air stability, compatibility with the electrode, electrochemical stability for high-voltage cathodes, and so on. Comprehensively fulfilling these aspects, halide SSEs are highly promising due to their stability in an oxygen atmosphere, flexibility with electrodes, and electrochemical stability at high voltages. Nevertheless, the low ionic conductivity of $\sim 10^{-4}$ S cm^{-1} even at high temperatures and hypersensitivity towards moisture remain constraints for most reported halide SSEs. In this work, we report a halide superionic conductor, Li_3InCl_6, with a high Li^+ conductivity of 1.49×10^{-3} S cm^{-1} at room temperature. Li_3InCl_6 is highly stable in ambient air and possesses high ionic conductivity retention after a reheating process. Furthermore, it is chemically and electrochemically stable when in direct contact with a high-voltage oxide cathode (*e.g.* $LiCoO_2$) without interfacial protection. Overall, the Li_3InCl_6 SSE owns essential advantages over the commercial sulfide SSEs in terms of air/humidity durability and compatibility with bare oxide cathodes, making it significantly attractive for practical applications.

All-solid-state lithium batteries (ASSLBs) with solid-state electrolytes (SSEs) are considered as a promising next-generation energy storage technology that can enable high theoretical energy densities.[1–4] The low ionic conductivity of SSEs was previously considered to be the main challenge for the development of ASSLBs. With significant progress over the years, many oxide and sulfide-based SSEs with high ionic conductivities around 10^{-3} S cm^{-1} have been developed, and some sulfide SSEs can even achieve values greater than 10^{-2} S cm^{-1} at room temperature.[5–9] Despite the great progress in achieving a high bulk conductivity, incorporation of these SSEs in ASSLBs has been difficult and the electrochemical performance is still inferior to their liquid electrolyte counterparts.

Generally, oxide SSEs possess good chemical stability and wide electrochemical windows. However, the stiffness and brittleness of oxide SSEs usually require a difficult fabrication process for the assembly of ASSLBs. High temperature sintering processes are needed for the preparation of electrode/oxide SSE composites, which can induce side-reactions between the electrode/oxide SSEs during the co-sintering process.[10,11] In contrast, sulfide SSEs are more attractive due to the ultra-high ionic conductivity and deformability. However, they still face considerable challenges including instability towards air/moisture, oxide cathodes, and externally applied voltages. Exposure to ambient air can lead to the generation of toxic H_2S gas, reduced ionic conductivity, and degradation of the chemical structure.[12] Direct integration of sulfide SSEs with cathode components results in large interfacial resistances caused by unavoidable side reactions, which is exacerbated by the decomposition of SSEs at high voltage.[13–15]

[a] Department of Mechanical and Materials Engineering, University of Western Ontario, 1151 Richmond St, London, Ontario, N6A 3K7, Canada. E-mail: xsun9@uwo.ca
[b] Canadian Light Source, 44 Innovation Boulevard, Saskatoon, SK S7N 2V3, Canada
[c] Department of Chemistry, University of Western Ontario, 1151 Richmond St, London, Ontario, N6A 3K7, Canada
[d] China Automotive Battery Research Institute Co. Ltd, 5th Floor, No. 43, Mining Building, North Sanhuan Middle Road, Beijing, 100088, China
[e] Glabat Solid-State Battery Inc., 700 Collip Circle, London, ON, N6G 4X8, Canada

† Electronic supplementary information (ESI) available. See DOI: 10.1039/c9ee02311a

‡ X. L. and J. L. contributed equally to the work.

Nevertheless, most of the aforementioned obstacles such as instability towards oxygen, electrodes, and low voltage range described above are no longer issues for halide SSEs.[16,17] Tetsuya Asano *et al.* reported halide Li_3YCl_6 and Li_3YBr_6 SSEs, which showed high room-temperature ionic conductivities of 1 mS cm^{-1}, good stability in dry-oxygen, and good compatibility with a $LiCoO_2$ cathode.[16] Wide electrochemical windows over 4 V for halide SSEs (*e.g.*, Li_3ErCl_6, Li_3GdCl_6) were predicted by Yifei Mo *et al.* using first principle calculations,[17] which are significantly wider than the current oxide and sulfide SSEs such as 1.75–3.71 V for $Li_{0.33}La_{0.56}TiO_3$, and 1.72–2.29 V for $Li_{10}GeP_2S_{12}$.[18,19] Good interface compatibility with oxide cathode materials both in pristine and delithiated forms were also proposed.[17] Besides, ultra-high Li^+ conductivity as high as 10 mS cm^{-1} at 300 K was predicted.[17] Unfortunately, most reported halide SSEs exhibit quite low ionic conductivities $\sim 10^{-4}$ S cm^{-1} even at high temperatures around 200 °C and phase instability (Table S1, ESI†).[20–27] Moreover, no halide SSEs have been reported to possess stability in ambient air due to their hypersensitivity towards moisture.[28]

In the present work, we report a halide Li^+ superionic conductor of Li_3InCl_6, which is stable towards oxide-based cathodes and is also stable in ambient air. The synthesized Li_3InCl_6 possesses good chemical stability towards traditional oxide cathode materials (*e.g.*, $LiCoO_2$) and a high ionic conductivity of 1.49 mS cm^{-1} at room temperature. The introduction of Li_3InCl_6 can effectively eliminate the side reactions between SSEs and cathode materials, and thus the battery performances are dramatically improved. Moreover, Li_3InCl_6 possesses good air stability, thermal stability, and recoverability after humidity exposure. X-ray photoelectron spectroscopy (XPS) and synchrotron X-ray absorption spectroscopy were utilized to study the stability of the Li_3InCl_6 structure after humidity exposure and with applied voltage.

The halide SSEs based on the Li–In–Cl system were synthesized mechanochemically from a stoichiometric mixture of binary compound precursors (LiCl and $InCl_3$) or followed by an annealing process (260 °C for 5 h). Fig. 1a shows the X-ray diffraction (XRD) patterns of the pristine ball milled-Li_3InCl_6 and annealed-Li_3InCl_6 samples. Both samples can be indexed well with a distorted monoclinic rock-salt structure with the *C*2/*m* space group (ICSD No. 04-009-9027). The ball milled sample exhibited broad Li_3InCl_6 peaks with low crystallinity after the ball-milling process. However, after annealing, the Li_3InCl_6 sample presented sharp XRD patterns, indicating its high crystallinity. It is apparent that only a low temperature of 260 °C is required for the annealing process, which is more energy sustainable than other halide SSEs obtained at high temperatures of over 550 °C.[16] Furthermore, as shown in Fig. S1 and S2 (ESI†), the two Li_3InCl_6 SSEs presented similar small particle sizes around several hundred nanometers, which were significantly smaller than the common sulfide SSE particles (usually around several microns),[29] and can possibly provide higher flexibility to accommodate the volume expansion of electrode materials.

The schematic structure of Li_3InCl_6 is presented in Fig. 1b and c, showing the cubic-closed-packed (ccp) arrangement of the Cl^- species. Similar to the reported halide SSEs such as Li_3YBr_6[16] and high temperature phase Li_3InBr_6,[30] the structure of annealed Li_3InCl_6 is essentially a distorted rock-salt LiCl structure. Particularly, one In^{3+} substitution could replace three Li^+ cations and introduce two intrinsic vacancies (V″). The octahedral interstitial sites are occupied by Li^+, In^{3+}, and vacancies in a ratio of 3 : 1 : 2. Presumably, these intrinsic vacancies are essential to the high ionic conductivity of the crystalline Li_3InCl_6, although the anion-close-packed structure possesses a relatively low-symmetry structure compared to the body-centered cubic-like arrangement of the anion sublattice

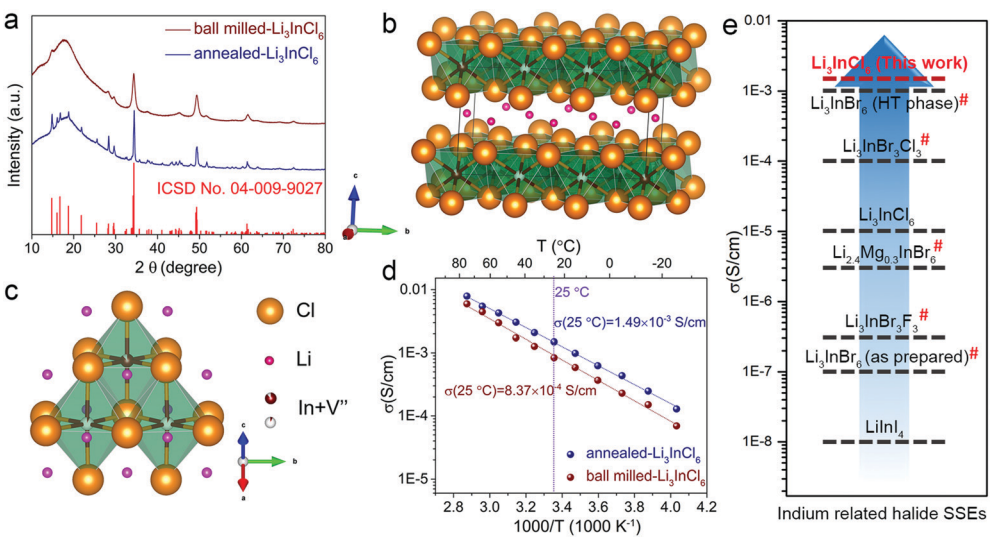

Fig. 1 (a) X-ray diffraction patterns of the as-prepared ball milled and annealed Li_3InCl_6 samples, along with the standard pattern of the previously reported Li_3InCl_6 (ICSD No. 04-009-9027). Structure of annealed-Li_3InCl_6. (b) Layered structure, showing two kinds of $InCl_6^{3-}$ octahedra with different occupations of In^{3+} (red wine) and vacancies (V″, white); orange balls are Cl^-. (c) Schematic unit showing typical Li^+ location around the $InCl_6^{3-}$ octahedra. (d) Arrhenius plots of ball-milled and annealed Li_3InCl_6 samples. (e) Summary of reported indium related halide SSEs.[24–27,33–36] HT phase means high-temperature phase, bromide-based SSEs marked with "#" face the problem of structure transition around −13 to 60 °C.

recently proposed for sulfide-based SSEs with high ionic conductivity.[31]

In halide SSE systems, there might be temperature related phase transitions from a high conductivity phase to a low conductivity phase, which hinders the feasibility of halide-based ASSLBs.[27,32] The phase stability and ionic conductivity of Li_3InCl_6 SSEs were evaluated over a wide range from −25 to 75 °C. Fig. 1d displays the Arrhenius plots for cells using the ball-milled Li_3InCl_6 and annealed-Li_3InCl_6, showing that the room-temperature ionic conductivity is 8.37×10^{-4} and 1.49×10^{-3} S cm^{-1}, respectively. The XRD patterns and ionic conductivities of other samples obtained with different annealing parameters are shown in Fig. S3 and S4 (ESI†). It is apparent that a higher annealing temperature or a longer annealing time is not required to achieve a pure Li_3InCl_6 phase with a high ionic conductivity. As presented in Fig. 1e, the room-temperature ionic conductivity of Li_3InCl_6 SSE in this work is the highest among the previous indium related halide-based SSEs.[24–27,33–36] Clearly, the acheived ionic conductivity values are much higher than that of $\sim 10^{-5}$ S cm^{-1} reported for Li_3InCl_6 in 1992.[34] Most of the bromide-based SSEs face the problem of strcuture transition around −13 to 60 °C, which makes them not suitable for practical applications (details are shown in Table S1, ESI†).

The electronic conductivities of the annealed-Li_3InCl_6 were measured by a direct current (DC) polarization measurement using a cell configuration of SS/Li_3InCl_6/SS (where SS refers to stainless steel disks) symmetric cells at room temperature. Fig. S5a (ESI†) shows the DC polarization curves of the annealed-Li_3InCl_6 at different voltages. Upon an applied voltage, the current initially responded with a large value and rapidly decayed in less than 2 s to a stabilized value on the order of 10^{-7} A. From a linear fit between DC voltage and stabilized current (Fig. S5b, ESI†), the DC electronic conductivities were estimated to be 5.4×10^{-9} S cm^{-1} for the annealed-Li_3InCl_6, which is 6 order of magnitude lower than its ionic conductivity at room temperature. The high ionic conductivity, relatively low electronic conductivity, and wide thermal stability windows of Li_3InCl_6 demonstrate great promise as a superionic conductive SSE for ASSLBs.

Processibility in air and recoverability for spoiled SSEs are important factors affecting the manufacturing cost. The dry air stability of annealed-Li_3InCl_6 was first tested by exposing the powder sample to a flow of dry air for 20 h at room temperature or with heating from room temperature to 450 °C at 5 °C min^{-1}. In both cases, the sample's weight was stable without any observable exothermic or endothermic peaks present in the TGA curves and differential scanning calorimetry (DSC) curves (Fig. 2a and Fig. S6, ESI†). The corresponding ionic conductivities and activation energies of Li_3InCl_6 SSEs with dry air exposure for 10 h at room temperature and heated to 300 °C were also measured as presented in Fig. S7 and Table S2 (ESI†), indicating the thermal stability of Li_3InCl_6 in dry air at high temperatures. After exposure to air with a humidity of 1% or ambient air with a humidity around 30% for 12 h, the structure of Li_3InCl_6 SSE changed together with a reduced ionic conductivity (Fig. S8, ESI†), while after reheating at 260 °C for 1 h under vacuum, the samples exhibited similar XRD patterns with the pristine Li_3InCl_6 SSE (Fig. 2b). The samples reheated after the exposure

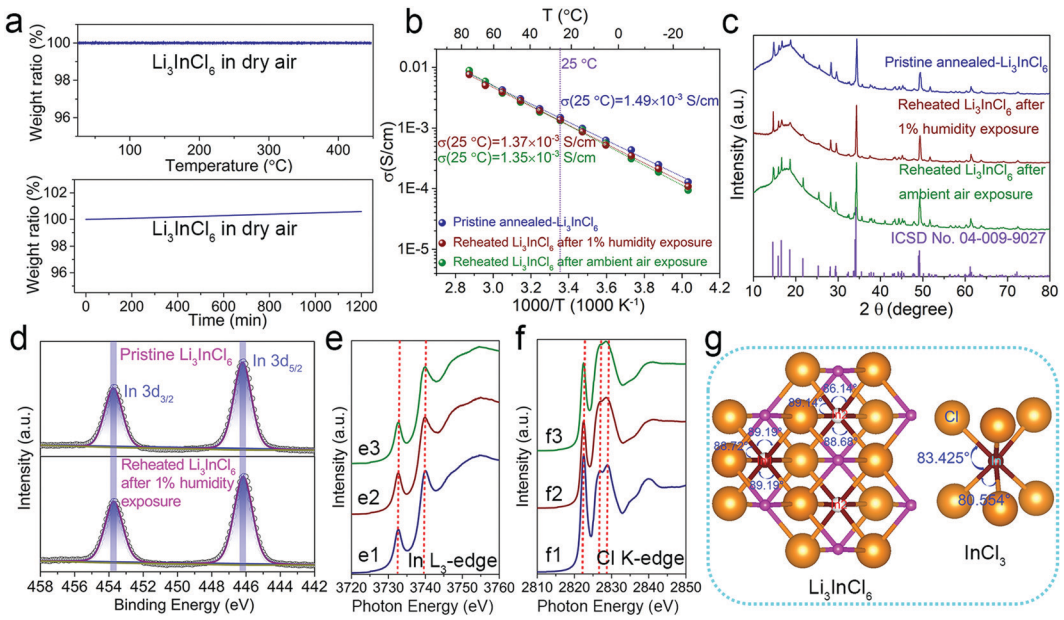

Fig. 2 Air stability of the annealed-Li_3InCl_6 SSE. (a) The TGA curves of the annealed-Li_3InCl_6 SSE sample in dry air atmosphere with heating from room temperature to 450 °C at 5 °C min^{-1} and resting at room temperature for 20 h. (b) Comparison of the ionic conductivities of annealed-Li_3InCl_6 SSE (blue), annealed-Li_3InCl_6 SSE after exposure to air with humidity of 1% (red) and ambient air with humidity around 30% (green) for 12 h and reheated at 260 °C for 1 h under vacuum. Corresponding structural evaluation of the treated Li_3InCl_6 SSEs by: (c) XRD patterns, and (d) XPS spectra. (e) Normalized In L_3-edge and (f) Cl K-edge XANES spectra of (e1 and f1) commercial $InCl_3$, (e2 and f2) pristine annealed-Li_3InCl_6, and (e3 and f3) reheated Li_3InCl_6 samples after exposure to air with a humidity of 1%. (g) Structures of Li_3InCl_6 and $InCl_3$.

show ionic conductivities of 1.37×10^{-3} and 1.35×10^{-3} S cm^{-1} at 25 °C, respectively, which were slightly lower than the pristine sample (1.49×10^{-3} S cm^{-1}), with only a marginal change in the activation energies being observed (Table S2, ESI†).

The stability of the Li_3InCl_6 SSEs was further proved by using XPS and X-ray absorption near-edge structure (XANES) analysis (Fig. 2d–f). The XPS spectra (Fig. 2d) of the fresh and humidity treated Li_3InCl_6 samples are almost the same, with the In $3d_{5/2}$ peak at 446.2 eV and In $3d_{3/2}$ peak at 453.8 eV, which is similar to the reported In^{3+}–Cl^-.[37,38] The collected In L_3-edge XANES spectra of the SSE together with that of commercial $InCl_3$ are presented in Fig. 2e. It was found that the annealed-Li_3InCl_6 and commercial $InCl_3$ showed very similar spectra in terms of shape and energy position. This should be due to the similar In^{3+} environment coordinated by six Cl^- forming octahedra for monoclinic Li_3InCl_6 and $InCl_3$ (Fig. 2g). The spectra showed an intense "white line" at 3732 eV due to 2p to localized s state transitions, as reported for InF_3.[39] Another shoulder peak is observed at 3740 eV (lower than the 3745.4 eV for InF_3 and 3744.6 eV for In_2O_3), which was likely due to the electronic transitions from the In 2p to unoccupied d states or 2p → 5s electronic transitions enhanced by s–d orbital hybridization.[39,40] For the Cl K-edge XANES spectra, in addition to the two typical peaks similar to the bulk LiCl at 2827 eV and 2829 eV,[41] the three spectra exhibited a pre-edge feature at 2822.5 eV (Fig. 2f), denoting electronic transitions from the Cl-1s shell to unoccupied orbitals with localized p character. The similarity of the XANES between $InCl_3$ and Li_3InCl_6 was attributed to their similar local symmetry as an octahedron with a central In and Cl ligands as presented in Fig. 2g. However, the pre-edge of the $InCl_3$ spectrum was much more intense compared to the spectra of the other two samples, which might be due to its distorted octahedral structure with different bond angles and the fact that the octahedra in Li_3InCl_6 exist with partial occupation of In with vacancies. Remarkably, the In L_3-edge and Cl K-edge spectra of reheated annealed-Li_3InCl_6 after exposure to an atmosphere with 1% humidity remain almost unchanged compared to the pristine one in terms of both spectral shape and energy position. Combined with the TGA, XRD, XPS, and ionic conductivity results, the annealed Li_3InCl_6 SSE demonstrated good air and humidity stability while retaining the high initial ionic conductivity.

To demonstrate the applicability of annealed-Li_3InCl_6 with the oxide cathode in ASSLBs, bulk-type ASSLBs with commercial bare $LiCoO_2$ cathodes were fabricated. The assembled ASSLBs consisted of a composite cathode layer of $LiCoO_2$ and Li_3InCl_6, and a thin compact layer of annealed-Li_3InCl_6 as a SSE layer tailoring the cathode layer; In foil was used as the anode (referred to as ASSLB with Li_3InCl_6 SSE, detailed information shown in ESI†). The SEM and energy dispersive X-ray (EDX) mapping images of the $LiCoO_2$–Li_3InCl_6 composite cathode showed good coverage of annealed-Li_3InCl_6 on $LiCoO_2$ (Fig. S9, ESI†). The thicknesses of the $LiCoO_2$–Li_3InCl_6 cathode layer and the Li_3InCl_6 SSE layer are about 100 μm and 320 μm, respectively (Fig. S10, ESI†). In comparison, another bulk-type ASSLB using $Li_{10}GeP_2S_{12}$ in both the cathode composite and the SSE layer (referred as ASSLB with $Li_{10}GeP_2S_{12}$ SSE) was fabricated.

Fig. 3a compares representative charge–discharge curves of the two ASSLBs at 0.1C (1C = 140 mA g^{-1}) between 1.9–3.6 V *vs.*

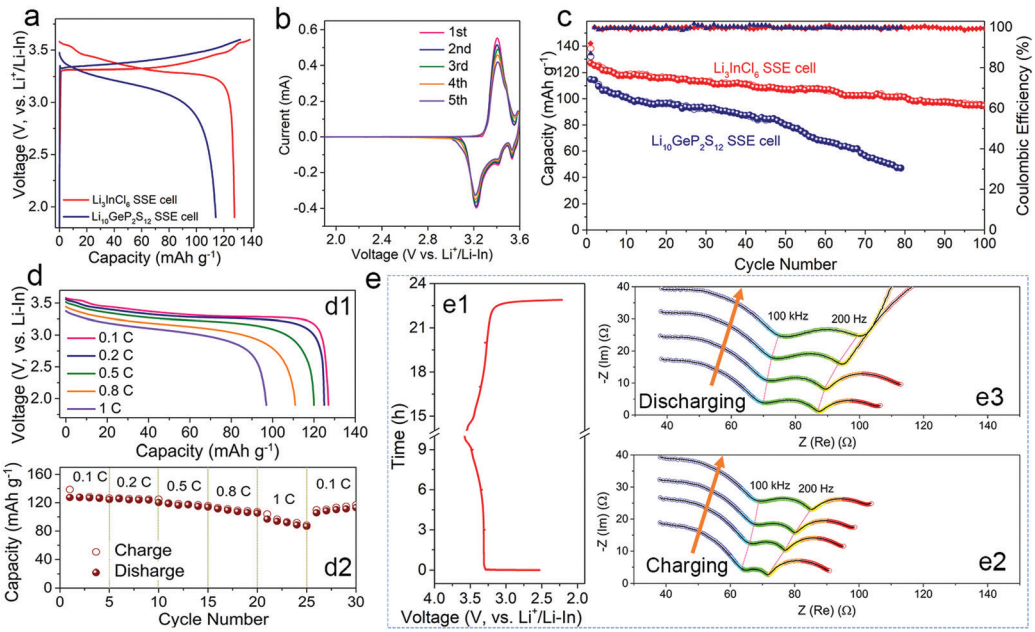

Fig. 3 Electrochemical performance of $LiCoO_2$–Li_3InCl_6/Li_3InCl_6/In all-solid-state cells at 25 °C. (a) Initial charge–discharge curves of $LiCoO_2$–Li_3InCl_6/Li_3InCl_6/In and $LiCoO_2$–$Li_{10}GeP_2S_{12}$/$Li_{10}GeP_2S_{12}$/In cells at 0.1C. (b) CV curves of $LiCoO_2$–Li_3InCl_6/Li_3InCl_6/In cells at 0.02 mV s^{-1}. (c) Cycling performance and coulombic efficiency of the $LiCoO_2$–Li_3InCl_6/Li_3InCl_6/In and $LiCoO_2$–$Li_{10}GeP_2S_{12}$/$Li_{10}GeP_2S_{12}$/In cells at 0.1C. (d) Rate capability of $LiCoO_2$–Li_3InCl_6/Li_3InCl_6/In cells at 0.1, 0.2, 0.5, 0.8 and 1C. (e) Impedance evolution of $LiCoO_2$–Li_3InCl_6/Li_3InCl_6/In cells during cycling. (e1) The charge–discharge curve of $LiCoO_2$–Li_3InCl_6/Li_3InCl_6/In cell cycled at 0.1C for 3 h and 2 h rest; (e2 and e3) corresponding impedance spectra recorded after 2 h rest during charging and discharging, respectively.

Li^+/LiIn (*i.e.*, 2.5–4.2 V *vs.* Li^+/Li) at room temperature. An initial discharge capacity of 127 mA h g^{-1} and a high initial coulombic efficiency of 92% were achieved by the ASSLB with the Li_3InCl_6 SSE. Remarkably, the ASSLBs using annealed-Li_3InCl_6 presented a very small overpotential and charge–discharge curves highly comparable to the $LiCoO_2$ cell using a typical liquid electrolyte (Fig. S11, ESI†). Moreover, the small plateaus at the end of charging and the beginning of discharging caused by the reversible phase transition of $LiCoO_2$ were observable in both the charge–discharge curves and cyclic voltammetry (CV) curves (Fig. 3b). This phenomenon indicated the feasible Li^+ transport across the interface between the bare $LiCoO_2$ and the annealed-Li_3InCl_6 SSE, which was observable in sulfide ASSLBs only when the $LiCoO_2$ was protected.[42] In contrast, the ASSLB with the $Li_{10}GeP_2S_{12}$ SSE showed severe polarization, a low reversible capacity of 114 mA h g^{-1}, and an inferior initial coulombic efficiency of 86% (Fig. 3a). The cycling performance of these ASSLBs at 0.1C is presented in Fig. 3c. Obviously, the cycling stability and reversible capacity of the ASSLB with the Li_3InCl_6 SSE are much more stable than those of the ASSLB with the $Li_{10}GeP_2S_{12}$ SSE, with a specific capacity of 95 mA h g^{-1} remaining after 100 cycles. Furthermore, the ASSLB with the Li_3InCl_6 SSE showed an acceptable rate capability as shown in Fig. 3d. Upon discharging at current densities of 0.1, 0.2, 0.5, 0.8, and 1C (with the same charging rate 0.1C), reversible capacities of 127, 125, 120, 111, and 97 mA h g^{-1} were achieved, respectively (Fig. 3d). Since the reversible capacity was recovered when returning to a lower current density, no severe isolation of the active material was inferred. The *in operando* impedance spectra were collected to monitor the impedance evolution of the ASSLB with the Li_3InCl_6 SSE in the first cycle. The cell was charged or discharged at 0.1C for 3 h and rested for 2 h before the impedance measurement. The charge–discharge curve shown in Fig. 3e1 is quite similar to that shown in Fig. 3a, and the minimal difference between the operating voltage and the open-circuit voltage again indicated the small polarization of the ASSLB with the Li_3InCl_6 SSE. The collected impedance spectra are shown in Fig. 3e2 and e3 with three obvious semicircles. Equivalent circuits of R(RQ)(RQ)Q (Fig. S12, ESI†) were used to fit the spectra, where the mid-frequency portion (colored green in the spectra) part was attributed to the interfacial resistance between $LiCoO_2$ and Li_3InCl_6 SSEs ($R_{SSE/LCO}$). The $R_{SSE/LCO}$ of the ASSLB with the Li_3InCl_6 SSE was one order of magnitude lower than that of the ASSLB with the $Li_{10}GeP_2S_{12}$ SSE (Fig. S13, ESI†). More specifically, the $R_{SSE/LCO}$ of the ASSLB with the $Li_{10}GeP_2S_{12}$ SSE increased to over 600 Ω after the first charge–discharge cycle, but the $R_{SSE/LCO}$ of the ASSLB with the Li_3InCl_6 SSE still maintained a value of ~17 Ω. The huge $R_{SSE/LCO}$ increase of the ASSLB with the $Li_{10}GeP_2S_{12}$ SSE was believed to be caused by the unavoidable side reactions between $LiCoO_2$ and $Li_{10}GeP_2S_{12}$ SSEs together with the structure destruction of $Li_{10}GeP_2S_{12}$ itself. In contrast, the slight increase in $R_{SSE/LCO}$ of the ASSLB with the Li_3InCl_6 SSE upon charge and discharge was likely due to the volume change of the active $LiCoO_2$ during cycling which induced cracks, leading to weakened contact within the composite cathode layer, as supported by the SEM images shown in Fig. S14 and S15 (ESI†). Moreover, the open circuit voltage (OCV) *vs.* time at 100% SOC curve shown in Fig. S16 (ESI†) further confirms the good stability of the ASSLB with the Li_3InCl_6 SSE.

The improved cycling stability and small impedance increase suggested good electrochemical stability of the annealed-Li_3InCl_6 SSE with the active $LiCoO_2$ cathode, showing no sign of SSE decomposition or side reactions. To verify this conclusion, XPS was performed to inspect the annealed-Li_3InCl_6 interface with $LiCoO_2$ at different charge/discharge status compared to the as-synthesized annealed-Li_3InCl_6 SSE. As shown in Fig. 4a, no obvious change in the In chemistry of the annealed-Li_3InCl_6 SSE was observed on the XPS spectra upon mixing with $LiCoO_2$ for weeks. Little change was observed after the electrochemical cycling, confirming the excellent chemical and electrochemical stabilities of the annealed-Li_3InCl_6 SSE with the layered oxide

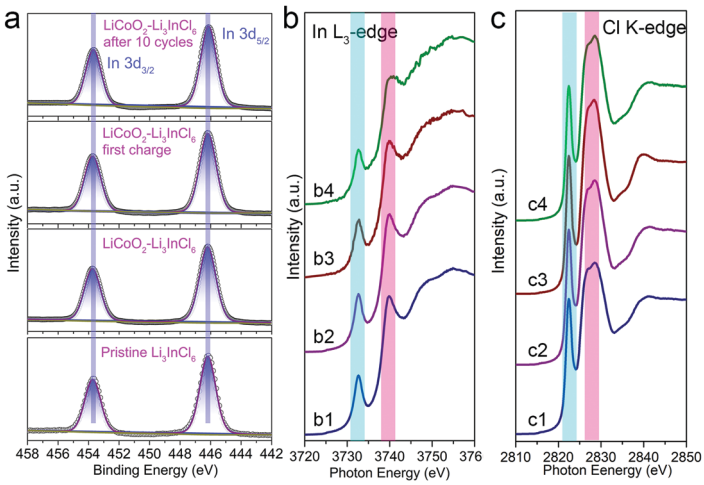

Fig. 4 (a) XPS spectra of the pristine annealed-Li_3InCl_6, $LiCoO_2$–Li_3InCl_6 cathode composites, $LiCoO_2$–Li_3InCl_6 cathode after first charge, and $LiCoO_2$–Li_3InCl_6 cathode after 10 cycles. (b) In L-edge and (c) Cl K-edge XANES spectra of (b1 and c1) pristine annealed-Li_3InCl_6, (b2 and c2) $LiCoO_2$–Li_3InCl_6 cathode composite, and $LiCoO_2$–Li_3InCl_6 cathode composites collected (b3 and c3) after first charge and (b4 and c4) after first discharge.

cathode $LiCoO_2$. Furthermore, the In L_3-edge and Cl K-edge XANES spectra for $LiCoO_2$–Li_3InCl_6 cathode composites at different charge/discharge status were collected (Fig. 4b and c). Consistent with the XPS results, the unchanged In L_3-edge and Cl K-edge spectra at fully charged or fully discharged states essentially confirmed the electrochemical stability of the annealed-Li_3InCl_6 SSE in contact with $LiCoO_2$ up to 4.2 V *vs.* Li^+/Li. The decreased intensity of the pre-edge peak for the Cl K-edge after charging/discharging and slight smooth-out of the doublet merely suggested an increase in disorder as noted above.

Conclusions

In summary, a halide Li_3InCl_6 SSE is successfully synthesized by mechanical and annealing approaches, which shows conductivities as high as 0.84 and 1.49 $\times$ 10^{-3} S cm^{-1} at room temperature, respectively. We demonstrate that Li_3InCl_6 is highly stable in ambient air and possesses an excellent ionic conductivity retention after a reheating process. More importantly, Li_3InCl_6 is stable in direct contact with high-voltage oxide cathode materials, yielding high-performance ASSLBs using Li_3InCl_6 with a $LiCoO_2$ cathode without any protective coating. Our results suggest that Li_3InCl_6 is a highly promising solid-state ionic conductor candidate for ASSLBs.

Author contributions

X. L. and J. L. designed and performed the experiments on material synthesis, characterization, and battery testing. M. B., W. L., X. L., Y. H., and T. S. contributed to the XAS experiments. C. W., S. D., C. Y., and F. Z. contributed to the data analysis. R. L. helped with the SEM images. X. L., J. L., J. L., and K. A. prepared the manuscript. L. Z., S. Z., S. L. and H. H. participated in the discussion of the data. All authors discussed the results and commented on the manuscript. X. S. supervised the work.

Conflicts of interest

There are no conflicts to declare.

Acknowledgements

This research was supported by the Natural Sciences and Engineering Research Council of Canada (NSERC), GLABAT Solid-State Battery Inc., China Automotive Battery Research Institute Co. Ltd, Canada Research Chair Program (CRC), Canada Foundation for Innovation (CFI), Ontario Research Fund, the Canada Light Source at University of Saskatchewan (CLS), Canada MITACS fellowships, and University of Western Ontario.

References

1 J. C. Bachman, S. Muy, A. Grimaud, H.-H. Chang, N. Pour, S. F. Lux, O. Paschos, F. Maglia, S. Lupart and P. Lamp, *Chem. Rev.*, 2015, **116**, 140–162.
2 Z. Zhang, Y. Shao, B. Lotsch, Y.-S. Hu, H. Li, J. Janek, L. F. Nazar, C.-W. Nan, J. Maier and M. Armand, *Energy Environ. Sci.*, 2018, **11**, 1945–1976.
3 S.-J. Tan, X.-X. Zeng, Q. Ma, X.-W. Wu and Y.-G. Guo, *Electrochem. Energy Rev.*, 2018, **1**, 113–138.
4 E. Umeshbabu, B. Zheng and Y. Yang, *Electrochem. Energy Rev.*, 2019, **2**, 199–230.
5 N. Kamaya, K. Homma, Y. Yamakawa, M. Hirayama, R. Kanno, M. Yonemura, T. Kamiyama, Y. Kato, S. Hama and K. Kawamoto, *Nat. Mater.*, 2011, **10**, 682.
6 Y. Seino, T. Ota, K. Takada, A. Hayashi and M. Tatsumisago, *Energy Environ. Sci.*, 2014, **7**, 627–631.
7 Y. Kato, S. Hori, T. Saito, K. Suzuki, M. Hirayama, A. Mitsui, M. Yonemura, H. Iba and R. Kanno, *Nat. Energy*, 2016, **1**, 16030.
8 M. A. Kraft, S. Ohno, T. Zinkevich, R. Koerver, S. P. Culver, T. Fuchs, A. Senyshyn, S. Indris, B. J. Morgan and W. G. Zeier, *J. Am. Chem. Soc.*, 2018, **140**, 16330–16339.
9 L. Nazar, P. Adeli, J. D. Bazak, K.-H. Park, I. Kochetkov, A. Huq and G. Goward, *Angew. Chem., Int. Ed.*, 2019, **58**, 8681–8686.
10 Y. Liu, Q. Sun, D. Wang, K. Adair, J. Liang and X. Sun, *J. Power Sources*, 2018, **393**, 193–203.
11 D. Wang, Q. Sun, J. Luo, J. Liang, Y. Sun, R. Li, K. Adair, L. Zhang, R. Yang and S. Lu, *ACS Appl. Mater. Interfaces*, 2019, **11**, 4954–4961.
12 T. Kimura, A. Kato, C. Hotehama, A. Sakuda, A. Hayashi and M. Tatsumisago, *Solid State Ionics*, 2019, **333**, 45–49.
13 R. Koerver, I. Aygün, T. Leichtweiß, C. Dietrich, W. Zhang, J. O. Binder, P. Hartmann, W. G. Zeier and J. R. Janek, *Chem. Mater.*, 2017, **29**, 5574–5582.
14 H. Visbal, Y. Aihara, S. Ito, T. Watanabe, Y. Park and S. Doo, *J. Power Sources*, 2016, **314**, 85–92.
15 G. Oh, M. Hirayama, O. Kwon, K. Suzuki and R. Kanno, *Chem. Mater.*, 2016, **28**, 2634–2640.
16 T. Asano, A. Sakai, S. Ouchi, M. Sakaida, A. Miyazaki and S. Hasegawa, *Adv. Mater.*, 2018, **30**, 1803075.
17 S. Wang, Q. Bai, A. M. Nolan, Y. Liu, S. Gong, Q. Sun and Y. Mo, *Angew. Chem., Int. Ed.*, 2019, **58**, 8039–8043.
18 Y. Zhu, X. He and Y. Mo, *ACS Appl. Mater. Interfaces*, 2015, **7**, 23685–23693.
19 W. D. Richards, L. J. Miara, Y. Wang, J. C. Kim and G. Ceder, *Chem. Mater.*, 2015, **28**, 266–273.
20 W. Schmidt and H. Lutz, *Ber. Bunsenges. Phys. Chem.*, 1984, **88**, 720–723.
21 R. Kanno, Y. Takeda, M. Mori and O. Yamamoto, *Chem. Lett.*, 1987, 1465–1468.
22 H. D. Lutz, K. Wussow and P. Kuske, *Z. Naturforsch. B*, 1987, **42**, 1379–1386.
23 H. Lutz, Z. Zhang and A. Pfitzner, *Solid State Ionics*, 1993, **62**, 1–3.
24 K. Yamada, K. Kumano and T. Okuda, *Solid State Ionics*, 2006, **177**, 1691–1695.
25 Y. Tomita, H. Matsushita, K. Kobayashi, Y. Maeda and K. Yamada, *Solid State Ionics*, 2008, **179**, 867–870.
26 Y. Tomita, H. Nishiyama, K. Kobayashi, Y. Kohno, Y. Maeda and K. Yamada, *ECS Trans.*, 2009, **16**, 137–141.

27 Y. Tomita, H. Matsushita, H. Yonekura, Y. Yamauchi, K. Yamada and K. Kobayashi, *Solid State Ionics*, 2004, **174**, 35–39.
28 A. Manthiram, X. Yu and S. Wang, *Nat. Rev. Mater.*, 2017, **2**, 16103.
29 W. J. Li, M. Hirayama, K. Suzuki and R. Kanno, *Solid State Ionics*, 2016, **285**, 136–142.
30 K. Yamada, K. Iwaki, T. Okuda and Y. Tomita, *Solid State Ionics: Trends in the New Millennium*, World Scientific, 2002, pp. 621–628.
31 Y. Wang, W. D. Richards, S. P. Ong, L. J. Miara, J. C. Kim, Y. Mo and G. Ceder, *Nat. Mater.*, 2015, **14**, 1026.
32 Y. Tomita, H. Matsushita, K. Kobayashi and K. Yamada, *Solid State Ionics: The Science and Technology of Ions in Motion*, World Scientific, 2004, pp. 985–990.
33 Y. Tomita, H. Yonekura, Y. Yamauchi, K. Yamada and K. Kobayashi, *Z. Naturforsch., A: Phys. Sci.*, 2002, **57**, 447–450.
34 H. J. Steiner and H. Lutz, *Z. Anorg. Allg. Chem.*, 1992, **613**, 26–30.
35 Y. Tomita, A. Fuji-i, H. Ohki, K. Yamada and T. Okuda, *Chem. Lett.*, 1998, 223–224.
36 K. Yamada, S. Matsuyama, Y. Tomita and Y. Yamane, *Solid State Ionics*, 2011, **189**, 7–12.
37 Y. Hu, D.-Y. Zhou, B. Wang, Z.-K. Wang and L.-S. Liao, *Appl. Phys. Lett.*, 2016, **108**, 153303.
38 Z.-Q. Wang, Z.-Y. Xiong, X.-J. Ma, Y. Zhang, P. Chen and C.-H. Gao, *Org. Electron.*, 2017, **44**, 110–114.
39 M.-O. Figueiredo, T. Silva, D. Oliveira and D. Rosa, *Minerals*, 2012, **2**, 426–434.
40 T. Sham, *Phys. Rev. B: Condens. Matter Mater. Phys.*, 1985, **31**, 1888.
41 M. Kiguchi, M. Katayama, G. Yoshikawa, K. Saiki and A. Koma, *Appl. Surf. Sci.*, 2003, **212**, 701–704.
42 W. Zhang, D. A. Weber, H. Weigand, T. Arlt, I. Manke, D. Schröder, R. Koerver, T. Leichtweiss, P. Hartmann and W. G. Zeier, *ACS Appl. Mater. Interfaces*, 2017, **9**, 17835–17845.